Impact of Nickel on Iridium-Ruthenium Structure and Activity for the Oxygen Evolution Reaction under Acidic Conditions

Supporting information

Erlend Bertheussen,[†,#] Simon Pitscheider,[†,#] Susan R. Cooper,[†,#] Rebecca Pittkowski,[‡] Katrine Louise Svane,[‡] Aline Bornet,[§] Erik M. Wisaeus,[†] Kirsten M. Ø. Jensen,[‡] Jan Rossmeisl,[‡] Matthias Arenz,[§] Christian Kallesøe,[†] and Christoffer M. Pedersen*[,†]

[†]Danish Technological Institute, Center for Functional Materials, 2630 Taastrup, Denmark

[‡]Department of Chemistry, University of Copenhagen, 2100 Copenhagen, Denmark

[§]Department of Chemistry, Biochemistry and Pharmaceutical Sciences, University of Bern, 3012 Bern, Switzerland

Contents

EDX analysis results

Table S1. Average compositions with standard deviations for all catalysts synthesized in this study, with and without the presence of Ni.

Name	**Catalyst loading wt.%**	**Ir loading wt.%**	**Ru loading wt.%**	**Ni loading wt.%**	**Relative Ni loading (wt.% in cat)**
without Ni	39.1 ± 2.3	32.3 ± 2.7	6.8 ± 0.4	-	-
with Ni	37.6 ± 2.5	30.4 ± 1.9	6 ± 0.6	1.2 ± 0.5	3.2 ± 1.4

Calculated XRD

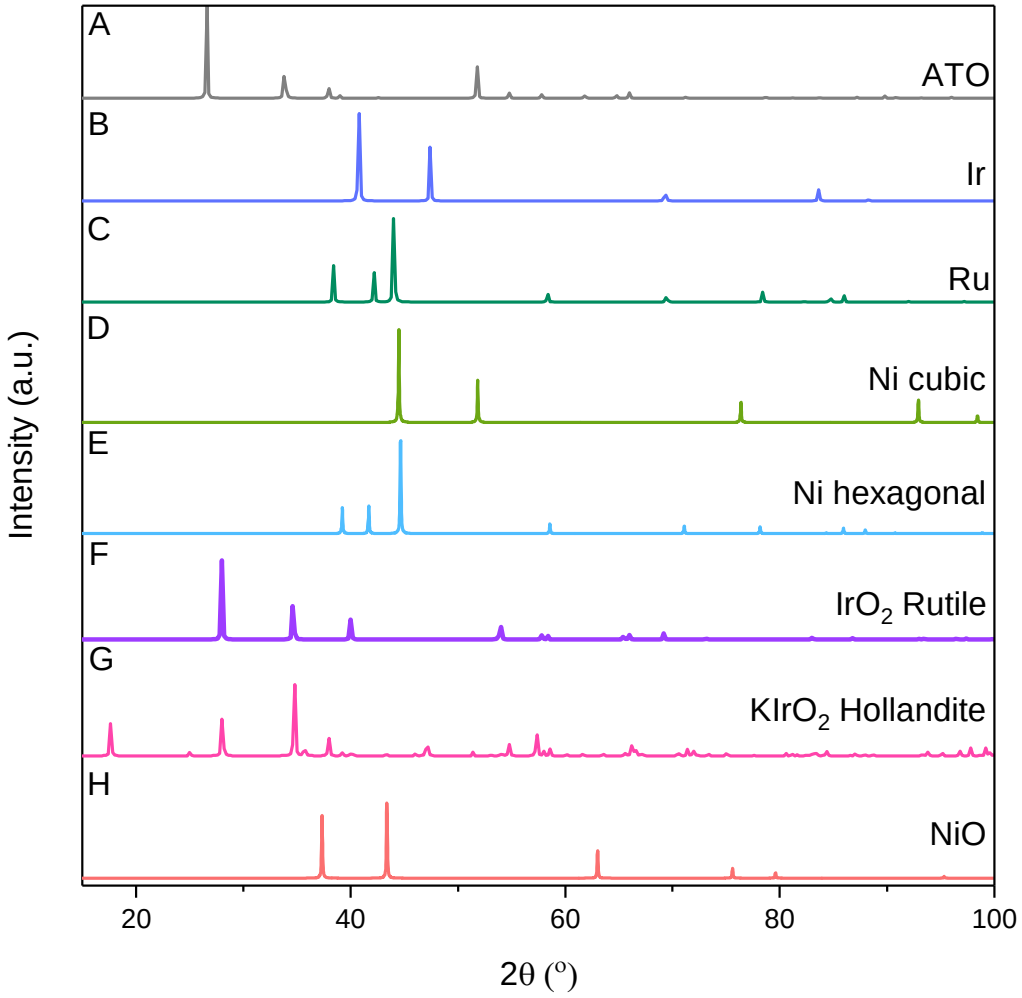

Figure S1. The calculated XRD patterns for possible materials synthesized for Ir or Ru particles on an ATO support. Rutile ATO that takes the space group P42/mnm[1] *is displayed in grey; metallic Ir that takes the space group Fm-3m*[2] *is displayed in blue; metallic Ru that takes the space group P63/mmc*[3] *is displayed in teal; metallic Ni can both take a cubic structure (space group Fm-3m*[4]*, in green) and hexagonal structure (space group P63/mmc*[3]*, in blue); rutile Ir oxide that takes the space group P42/mnm*[5] *in purple; hollandite Ir oxide that takes the space group I4/m*[6] *is displayed in pink; NiO that takes the space group Fm-3m*[7] *is displayed in orange. XRD powder patterns were calculated using Mercury 2021.2.0.*

XRD and Rietveld Refinement

ATO Rietveld refinement

Table S2. Refinement results for two different ATO samples. ATO samples were refined with a cassiterite phase that takes the space group P42/mnm.[1] *Both samples were flowed through the reactor without metal precursor salts at reaction temperature and pressure.*

	ATO 1	ATO 2
R_{Bragg}	1.67	5.09
Cassiterite a,b Å	4.740 Å	4.740 Å
Cassiterite c Å	3.188 Å	3.188 Å
Cassiterite Diameter nm	14 nm	15 nm
Cassiterite U	0.371	0.332
Cassiterite W	0.381	0.342

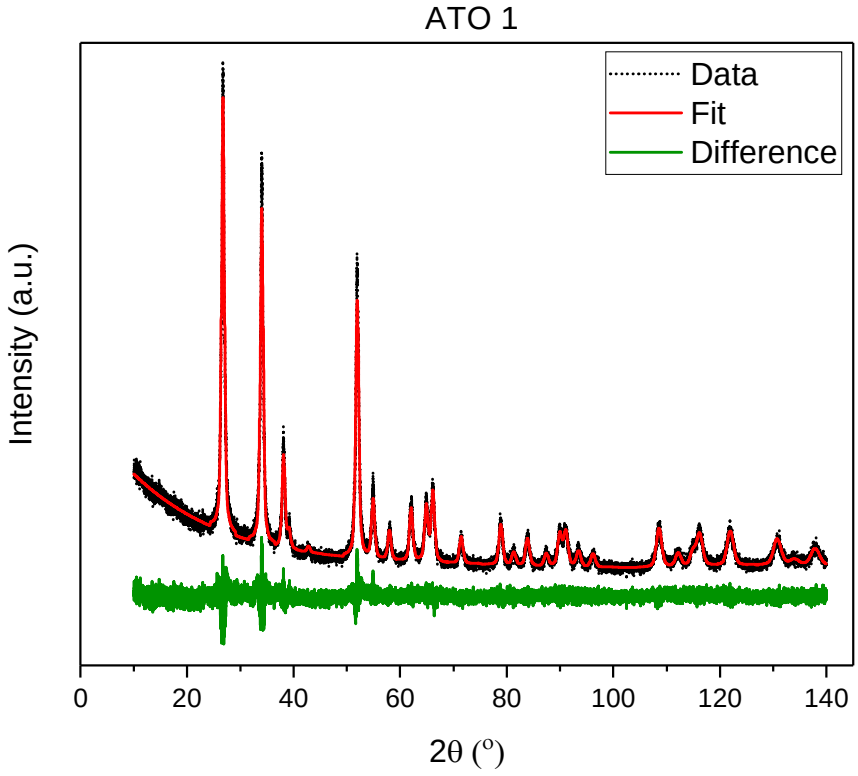

Figure S2. Refinement results for ATO 1.[1,8] *The data is shown as a black dashed line, the refinement fit is in red, and the difference between data and fit is in green. Refinements were done in Highscore plus v. 3.0.5.*

IrRu Rietveld refinement

Table S3. Refinement results for two different IrRu catalysts supported on ATO. IrRu samples were fit with a cassiterite phase that takes the space group P42/mnm[5] *and an iridium phase that takes the space group Fm-3m.*[2,3]

	IrRu 1	IrRu 2
R_{Bragg} Cassiterite	2.5	4.0
Cassiterite a,b Å	4.740 Å	4.740 Å
Cassiterite c Å	3.188Å	3.187 Å
Cassiterite Diameter nm	13 nm	13 nm
Cassiterite U	0.432	0.445
Cassiterite W	0.441	0.458
R_{Bragg} Iridium	3.9	4.1
Iridium a, b Å	3.837 Å	3.842 Å
Iridium Diameter nm	3 nm	3 nm
Iridium U	10.0	10.0
Iridium W	10.0	10.0

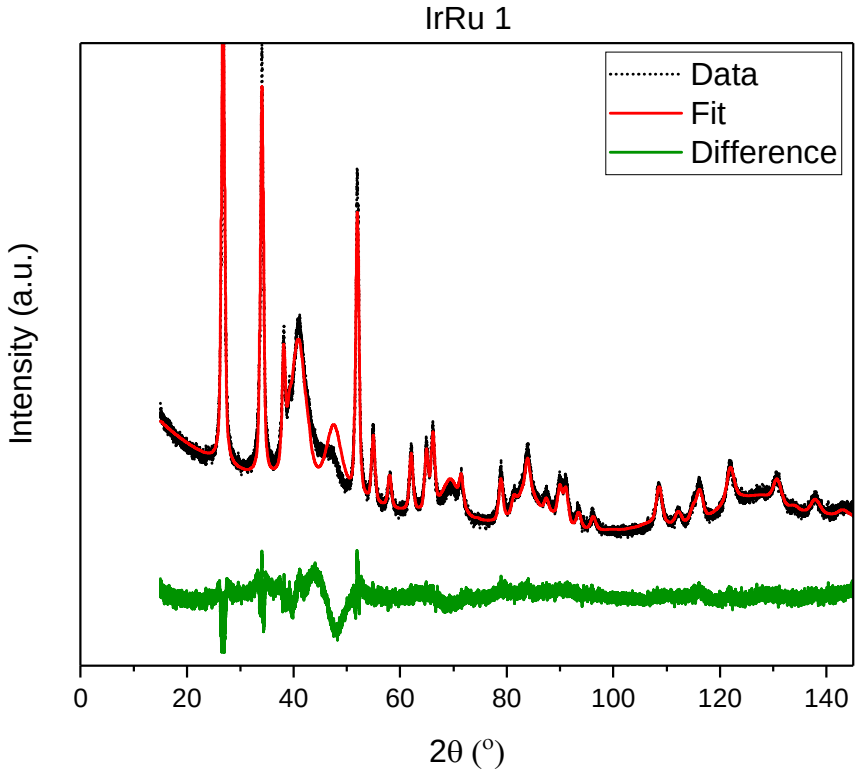

Figure S3. Refinement results for IrRu sample 1. The data is shown as a black dashed line, the refinement fit is in red, and the difference between data and fit is in green. Refinements were done in Highscore plus v. 3.0.5.

IrRuNi Rietveld refinement

Table S4. Refinement results for three different IrRuNi samples. IrRuNi samples were refined with a cassiterite phase that takes the space group P42/mnm.

	IrRuNi 1	IrRuNi 2	IrRuNi 3
R_{Bragg}	5.65	4.9	5.3
Cassiterite a,b Å	4.738 Å	4.738 Å	4.739 Å
Cassiterite c Å	3.185 Å	3.185 Å	3.186 Å
Cassiterite Diameter nm	12 nm	11 nm	12nm
Cassiterite U	0.551	0.644	0.523
Cassiterite W	0.561	0.654	0.533

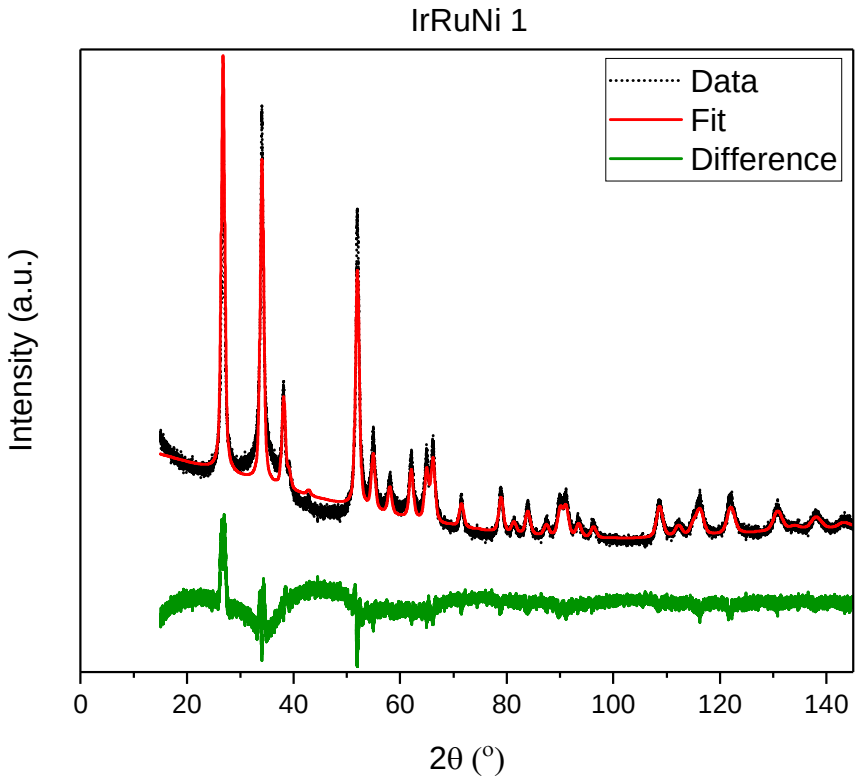

Figure S4. Refinement results for IrRuNi sample 1. The data is shown as a black dashed line, the refinement fit is in red, and the difference between data and fit is in green. Refinements were done in Highscore plus v. 3.0.5.

PDF data analysis

d-PDFs

To obtain signal from only the supported catalyst and not the support, ATO was used as a background for subtraction in Q space. Below are the f(Q) data of ATO, supported catalyst and difference curves after subtraction of ATO. It can be seen there are still some remaining peaks from ATO. Further subtraction led to split peaks at the ATO peak. This indicates that the remaining ATO peaks are broader than those from the support ATO.

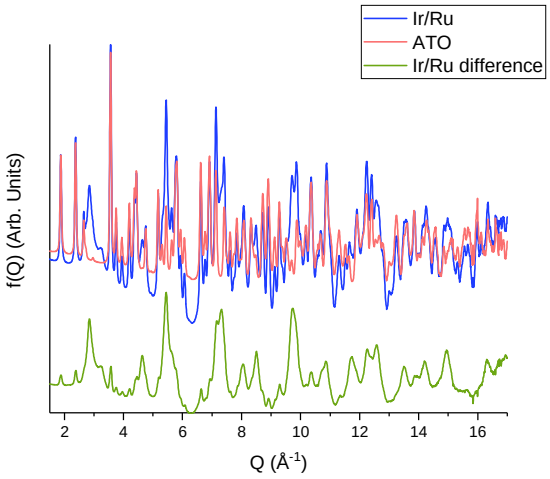

Figure S5. f(Q) of IrRu before and after subtraction of the ATO support. ATO f(Q) (orange), IrRu supported particles on ATO (blue), and the difference between the two (green).

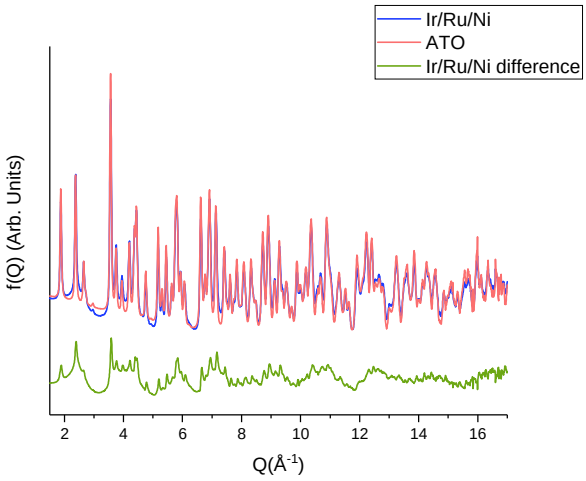

Figure S6. f(Q) of IrRuNi before and after subtraction of the ATO support. ATO f(Q) (orange), IrRuNi supported particles on ATO (blue), and the difference between the two (green).

Calculated PDF

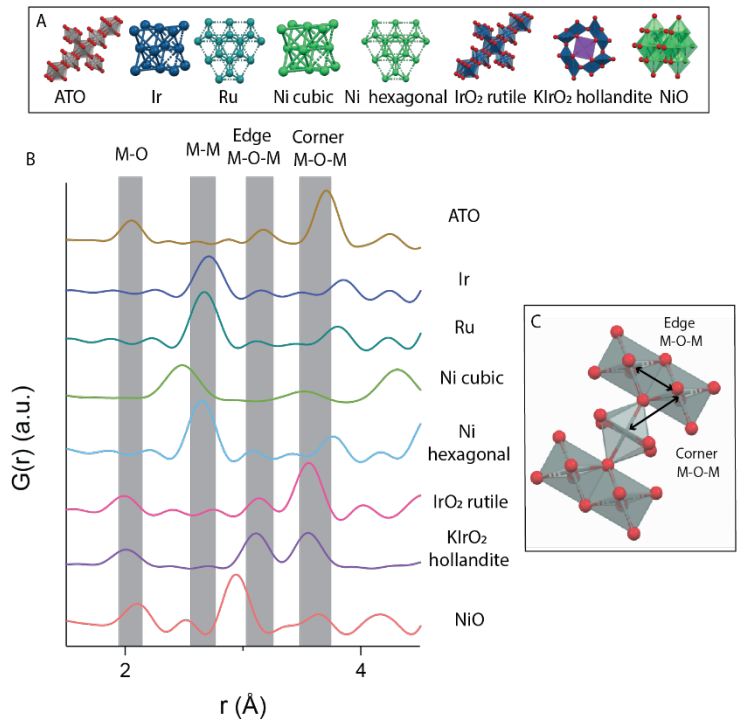

Figure S7. Structures of the possible materials synthesized for IrRu particles on an ATO support. A) From left to right: Rutile ATO that takes the space group P42/mnm,[1] *metallic iridium that takes the space group Fm-3m,*[2] *metallic ruthenium that takes the space group P63/mmc,*[3] *metallic nickel that takes the cubic space group Fm-3m, metallic nickel that takes the hexagonal space group P63/mmc, rutile iridium oxide that takes the space group P42/mnm,*[5] *hollandite iridium oxide that takes the space group I4/m,*[6,9] *and NiO that takes the space group Fm-3m.*[7] *Figures were made with Mercury 2021.2.0*[10]*. B) Calculated d-PDFs for the aforementioned structures. C) Difference between edge-sharing and corner-sharing octahedra.*

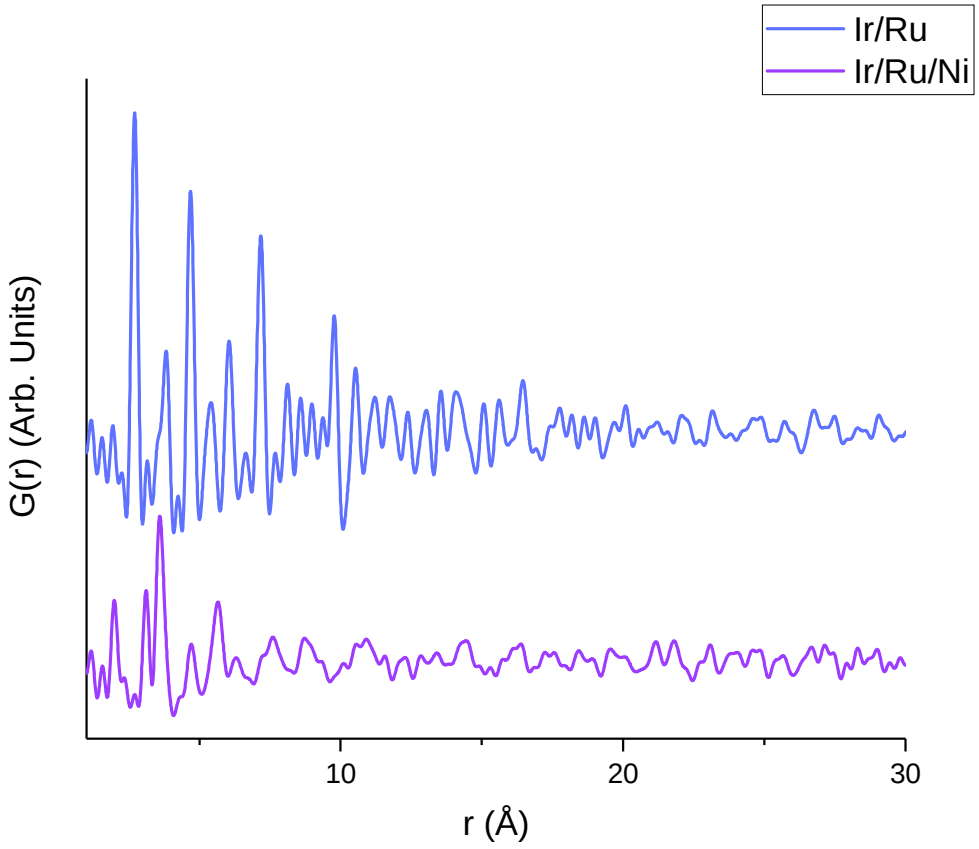

Figure S8. d-PDF of IrRu and IrRuNi particles from 1.5-30 Å.

ATO PDF and fit

PDFs were generated using xPDFsuite both with Kapton as a background for the ATO support. This was done in duplicate to ensure reproducibility. Data was fit from 1.5 – 60 Å. ATO was fit with SnO_2 cassiterite phase that takes the rutile structure with space group P42/mnm.[1]

Table S5. Refined results of data collected from an ATO sample fit with SnO_2 cassiterite phase that takes the rutile structure. The two refinements are from different powder samples that were flowed through the reactor without Ir or Ru reactants.

	ATO 1	ATO 2
R_W	0.120	0.105
a,b Å	4.734 Å	4.734 Å
c Å	3.184 Å	3.184 Å
Delta 2 Å	2.8 Å	2.7 Å
Diameter nm	11 nm	12 nm
Sn Uiso $Å^{-2}$	0.004 $Å^{-2}$	0.005 $Å^{-2}$
O Uiso $Å^{-2}$	0.028 $Å^{-2}$	0.028 $Å^{-2}$

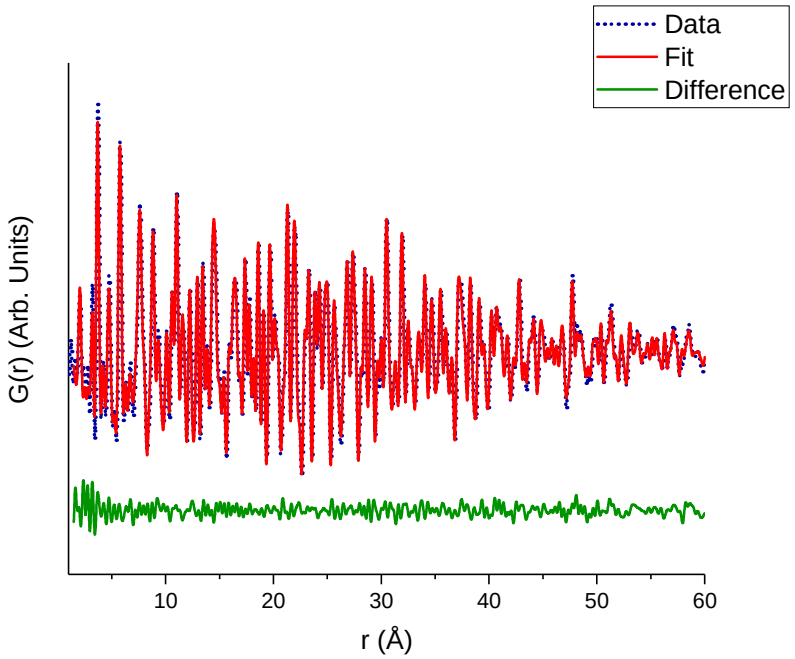

Figure S9. Representative fit of ATO with the cassiterite SnO_2 phase that takes the rutile structure that takes the space group P42/mnm. Refinement values are in Table S5.

IrRu fit to d-PDF

Table S6. Real-space refinement results for two different IrRu catalysts supported on ATO. ATO was subtracted out of the signal in Q-space. IrRu samples were fit with an iridium phase that takes the space group Fm-3m[2,3]. Fits were performed in the r-range from 1.5 Å – 30 Å using PDFgui.

	IrRu 1	IrRu 2
R_W	0.27	0.29
a Å	3.83 Å	3.83 Å
Delta 2 Å	5.1 Å	5.6 Å
Diameter nm	2 nm	3 nm
Ir Uiso $Å^{-2}$	0.007 $Å^{-2}$	0.007 $Å^{-2}$

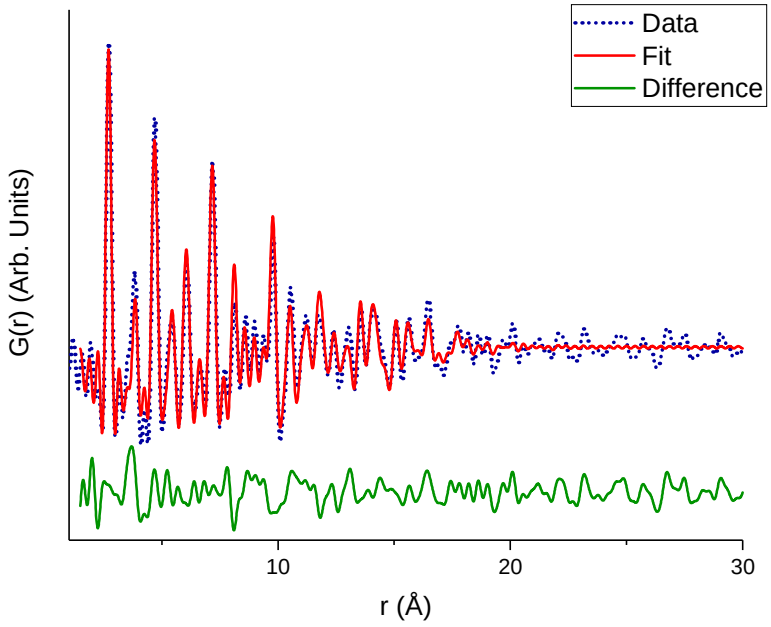

Figure S10. Representative real-space refinement results for an IrRu catalyst supported on ATO. ATO was subtracted out of the signal in Q-space. IrRu samples were fit with an iridium phase that takes the space group Fm-3m[2,3]. Refinement values are in Table S6.

IrRuNi fit to d-PDF

Table S7. Real-space refinement results for three different IrRuNi catalysts supported on ATO. ATO was subtracted out of the signal in Q-space. IrRuNi samples were fitted with an iridium oxide phase that takes the space group P42/mnm[2,3]. Fits were performed in two different r-ranges, from 1.5 Å – 30 Å and from 7-60 Å, using PDFgui.

	IrRuNi 1		IrRuNi 2		IrRuNi 3	
Fit range	1.5-30 Å	7-60 Å	1.5-30 Å	7-60 Å	1.5-30 Å	7-60 Å
R_W	0.55	0.37	0.54	0.36	0.54	0.33
a,b Å	4.643 Å	4.713 Å	4.635 Å	4.715 Å	4.640 Å	4.716 Å
c Å	3.119 Å	3.161 Å	3.116 Å	3.161 Å	3.117 Å	3.161 Å
Diameter nm	1 nm	10 nm	1 nm	9 nm	1 nm	10 nm
Ir Uiso $Å^{-2}$	0.009 $Å^{-2}$	0.011 $Å^{-2}$	0.008 $Å^{-2}$	0.010 $Å^{-2}$	0.009 $Å^{-2}$	0.011 $Å^{-2}$

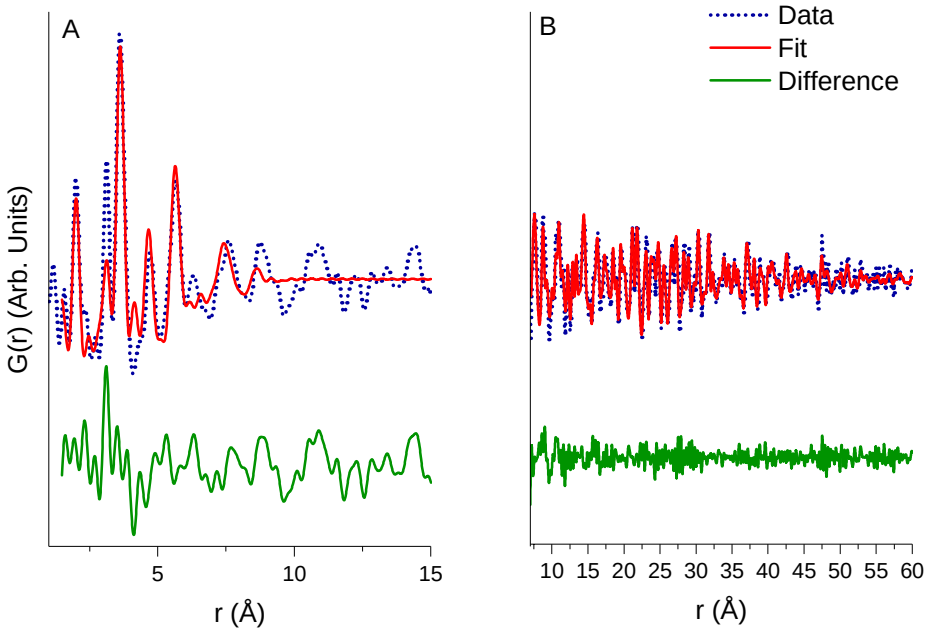

Figure S11. Real-space refinement of IrRuNi catalysts supported on ATO. ATO was subtracted out of the signal in Q-space. IrRuNi samples were fitted with an iridium oxide phase that takes the space group P42/mnm[2,3] fit from A) 1.5 Å – 30 Å, and B) is a fit from 7 Å – 60 Å. Refinement values are in Table S7.

Table S8. Real-space refinement results for an IrRuNi catalysts supported on ATO. ATO was subtracted out of the signal in Q-space. IrRuNi sample were fitted with an iridium oxide phase that takes the space group[2,3] I4/m.

	IrRuNi 1
Fit range	1.5-30 Å
R_W	0.61
a,b Å	10.42 Å
c Å	3.094 Å
Diameter nm	1 nm
Ir Uiso $Å^{-2}$	0.009 $Å^2$

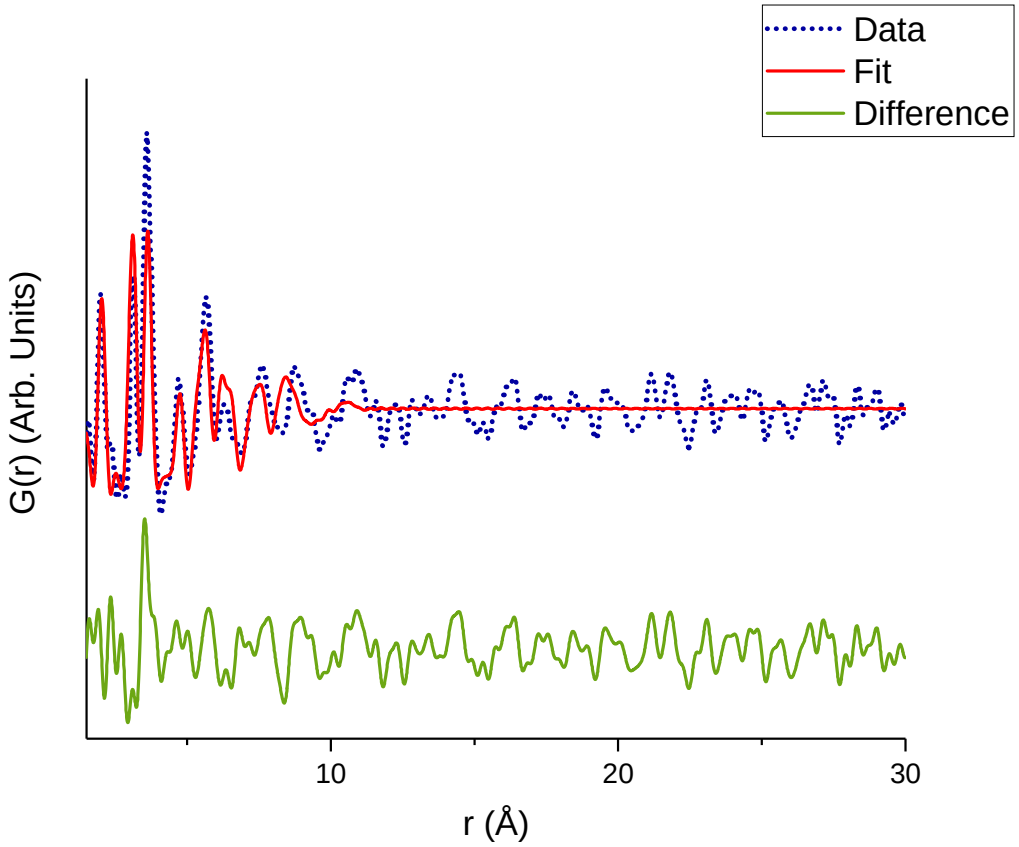

Figure S12. Real-space refinement of IrRuNi catalysts supported on ATO. ATO was subtracted out of the signal in Q-space. IrRuNi samples were fit with an iridium oxide phase that takes the space group I4/m[2,3] *fit from 1.5 Å – 30 Å.*

Transmission electron microscopy

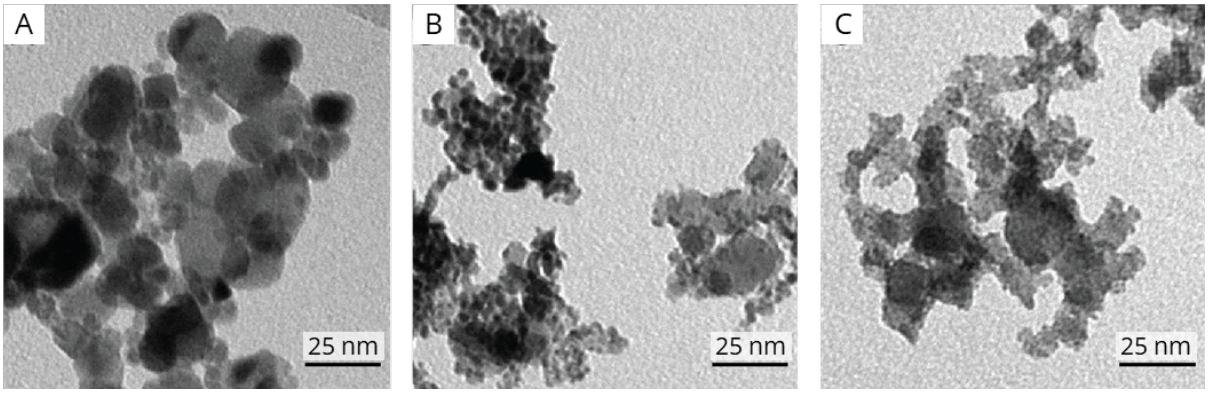

Figure S13. TEM micrographs for representative samples of (A) bare ATO, (B) IrRu nanoparticles on ATO, and (C) IrRuNi nanoparticles on ATO. Scale bar: 25 nm.

XAS data analysis

Parameters obtained for EXAFS data fitting of the IrRu sample (upper table) as well as IrRuNi samples (lower table), on both the Ru K-edge and the Ir L_{III}-edge (lower table), respectively, that show the coordination numbers (N), atomic bond length (R), Debye Waller factors (mean squared bond length disorder) (σ^2), absorption edge energy (E_0), and R_f-factor as a measure of fit quality.

Table S9. Parameters obtained for EXAFS data fitting of the IrRu sample – Fit with an fcc metal phase and a distorted octahedral oxygen coordination.

Sample	bond	N	R / Å	σ^2 / Å^2	E_0 / eV	R_f
Ru-edge	Ru-O_1	0.6 ± 0.2	1.82(2)	0.008(2)	22118 ± 1	0.011
	Ru-O_2	2.8 ± 0.7	2.00(1)	0.008(2)		
	Ru-Ru_1	3.3 ± 0.3	2.68(1)	0.004(3)		
	Ru-Ir_1	3.9 ± 0.4	2.68(1)	0.004(3)		
Ir-edge	Ir-O_1	1.0 ± 0.5	1.97(1)	0.005(3)	11224 ± 1	0.003
	Ir-O_2	1.2 ± 0.3	2.00(1)	0.005(3)		
	Ir-Ru_1	1.0 ± 0.1	2.68(3)	0.005(1)		
	Ir-Ir_1	6.2 ± 0.2	2.70(1)	0.005(1)		

Table S10. Parameters obtained for EXAFS data fitting of the IrRuNi sample – Fit with a hollandite metal oxide structure.

Sample	bond	N	R / Å	σ^2 / Å^2	E_0 / eV	R_f
Ru-edge	Ru-O_1	1.9 ± 0.4	1.84(7)	0.005(2)	22124 ± 3	0.021
	Ru-O_2	2.9 ± 0.5	2.01(2)	0.005(2)		
	Ru-Ru_1	2.0 ± 0.3	3.15(6)	0.001(6)		
	Ru-Ru_2	1.6 ± 0.6	3.31(8)	0.001(6)		
Ir-edge	Ir-O_1	2.4 ± 0.3	1.94(1)	0.001(2)	11230 ± 2	0.005
	Ir-O_2	3.5 ± 0.3	2.05(1)	0.001(2)		
	Ir-Ir_1	2.0 ± 0.5	3.07(3)	0.005(4)		
	Ir-Ir_2	2.0 ± 0.7	3.19(2)	0.005(4)		

Electrochemical measurements

Chronoamperometry OER activity measurements

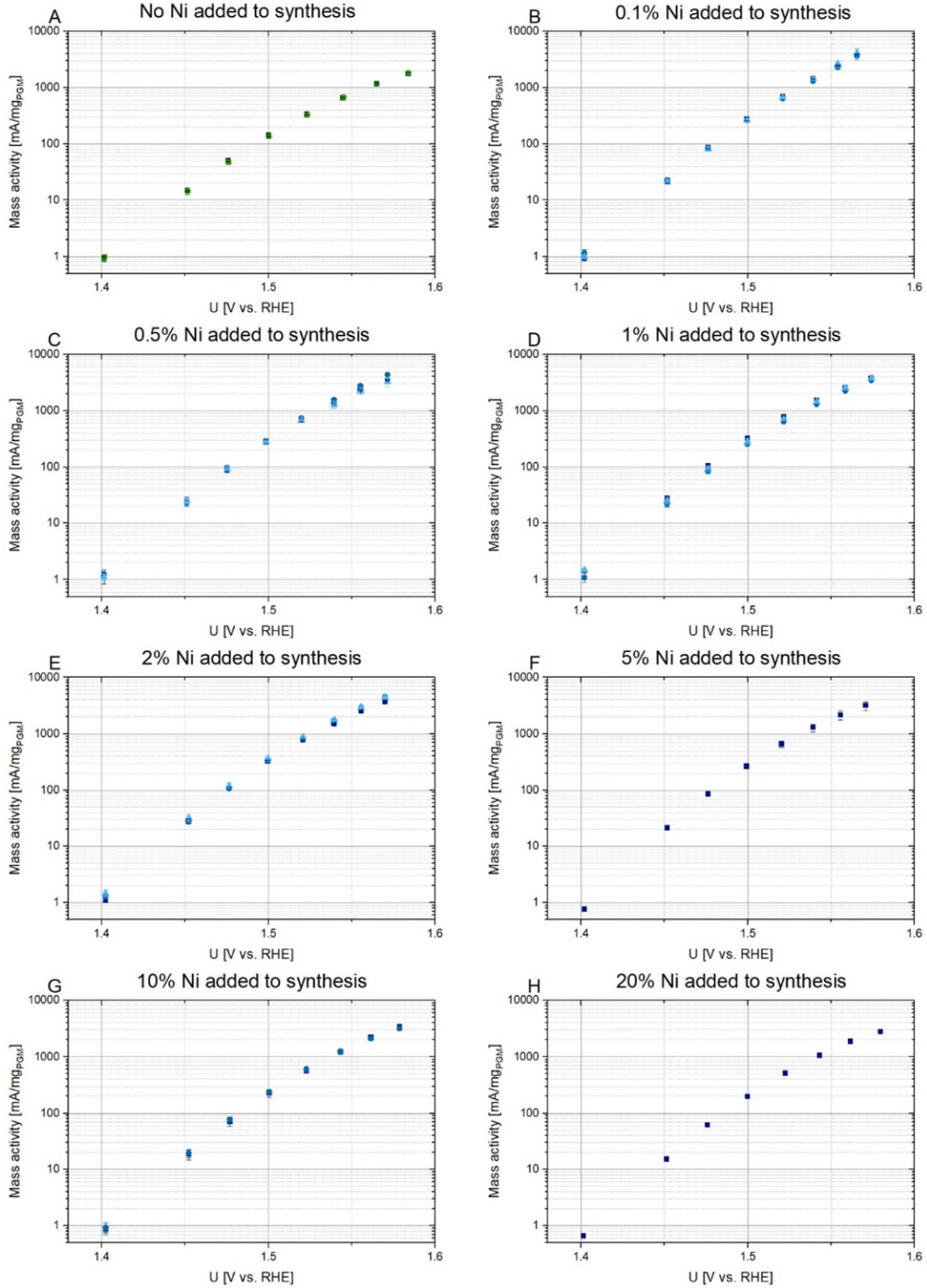

Figure S14. Chronoamperometry measurements of OER mass activity for representative samples of (A) an IrRu catalyst and (B-H) various IrRuNi catalysts with different amounts of Ni added during synthesis. Measurements were performed in N_2-saturated 0.1 M $HClO_4$ using an RDE setup.

Cyclic voltammetry

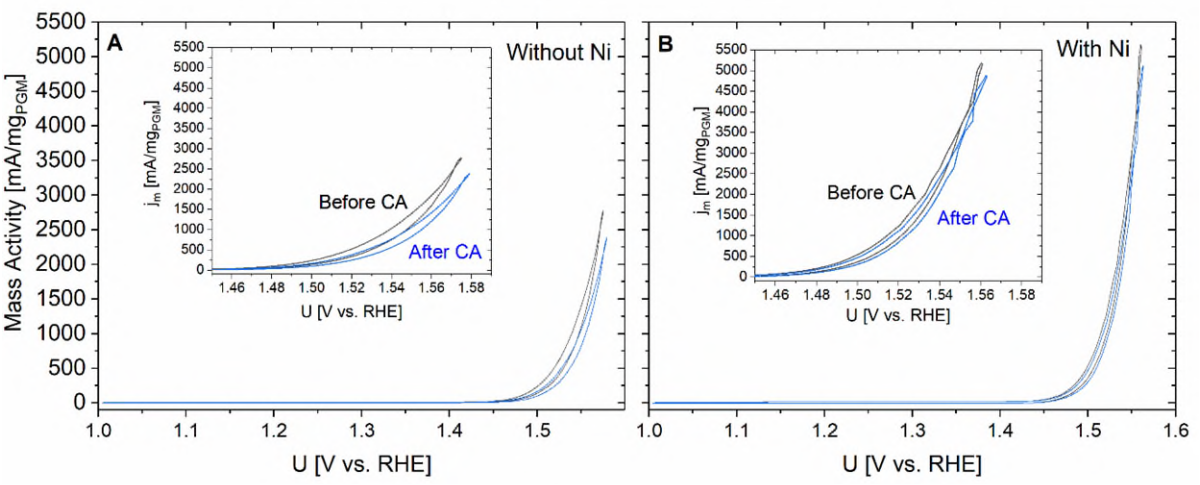

Figure S15. CV measurements of representative $Ir_{0.7}Ru_{0.3}$/ATO catalysts (A) without and (B) with Ni added during synthesis. The inset shows the relevant potential region where OER takes place. Cycle 5 of 5 performed before chronoamperometry (CA) measurements are shown in black, while cycle 3 of 3 performed after CA are shown in blue. Measurements were performed in N_2-saturated 0.1 M $HClO_4$ using an RDE setup.

CV measurements were performed before and after the CA activity evaluation, with representative measurements of a catalyst without and with Ni shown in Figure S15A and S15B, respectively. Some deactivation can be observed by comparing before and after, which is probably due to either corrosion of the glassy carbon support or the formation of gas bubbles in the catalyst layer during testing blocking some of the active sites.[11] This is, however, unlikely to have a strong impact on the results, since the same measurement protocol was used for all measurements reported in this study. If anything, the Ni-containing catalyst in Figure S15B appears more stable than the one without Ni.

Electrochemical Impedance Spectroscopy

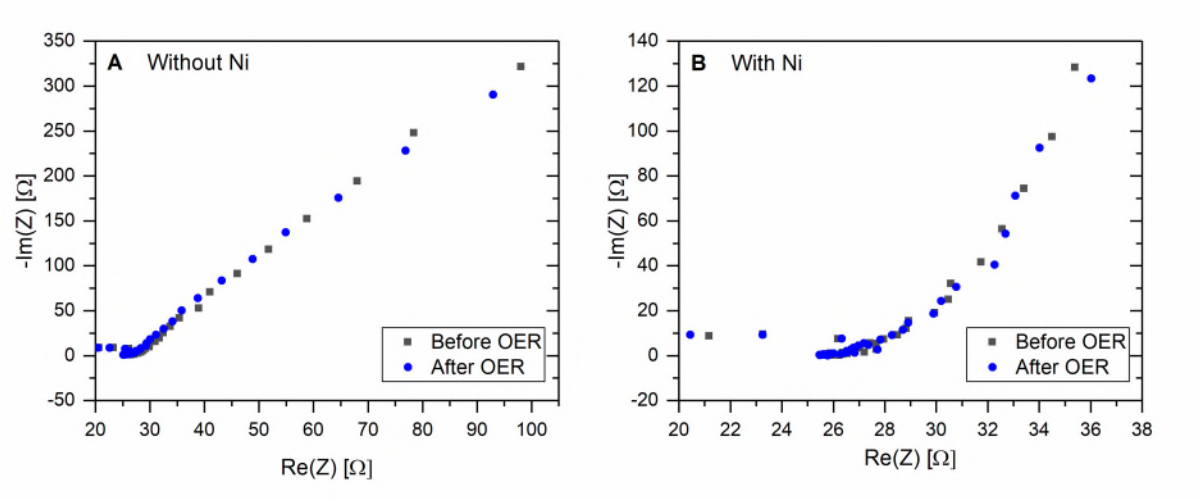

Figure S16. Electrochemical impedance spectroscopy of representative $Ir_{0.7}Ru_{0.3}$/ATO catalysts (A) without and (B) with Ni added during synthesis. Measurements were performed in N_2-saturated 0.1 M $HClO_4$ using an RDE setup.

Double layer capacitance analysis

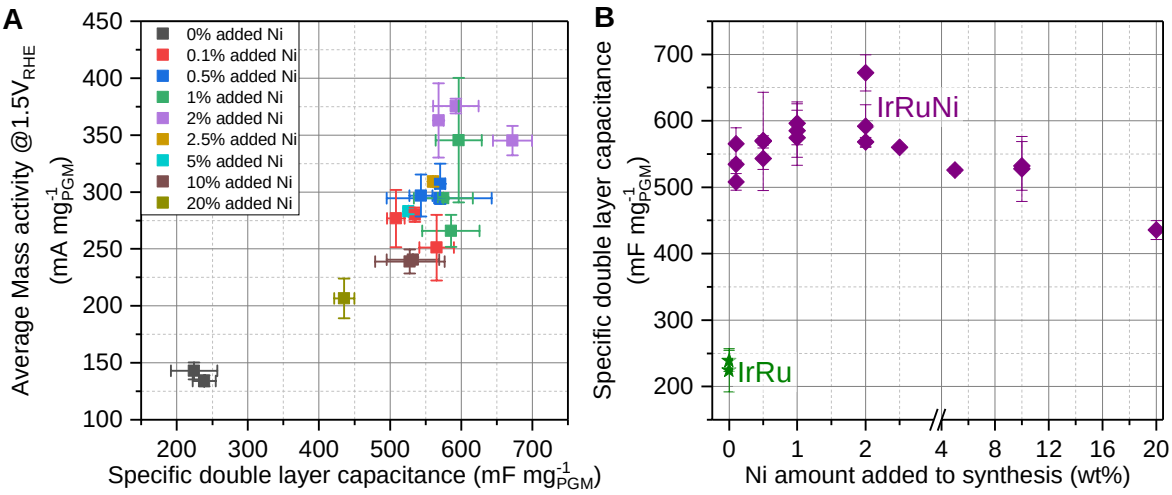

Figure S17. A) Correlation between the double layer capacitance (established in the non-faradaic area of the last CV scan before the CA for each sample in this study) and the average mass activity of the same samples. B) Correlation between the added Ni amount in the synthesis and the double layer capacitance.

Acid wash experiments

Table S11. Composition of two representative catalysts before and after acid wash in 0.1 M $HClO_4$ for at least 24 hours.

Catalyst name	Catalyst loading (wt.%)	Ir loading (wt.%)	Ru content (wt.%)	Ni content (wt.%)
R169 after synthesis	36.2	29.3	5.9	1.0
R169 after acid wash	36.2	29.4	5.9	0.9
R180 after synthesis	36.6	29.9	5.5	1.2
R180 after acid wash	36.7	29.4	5.7	1.6

DFT reaction pathways

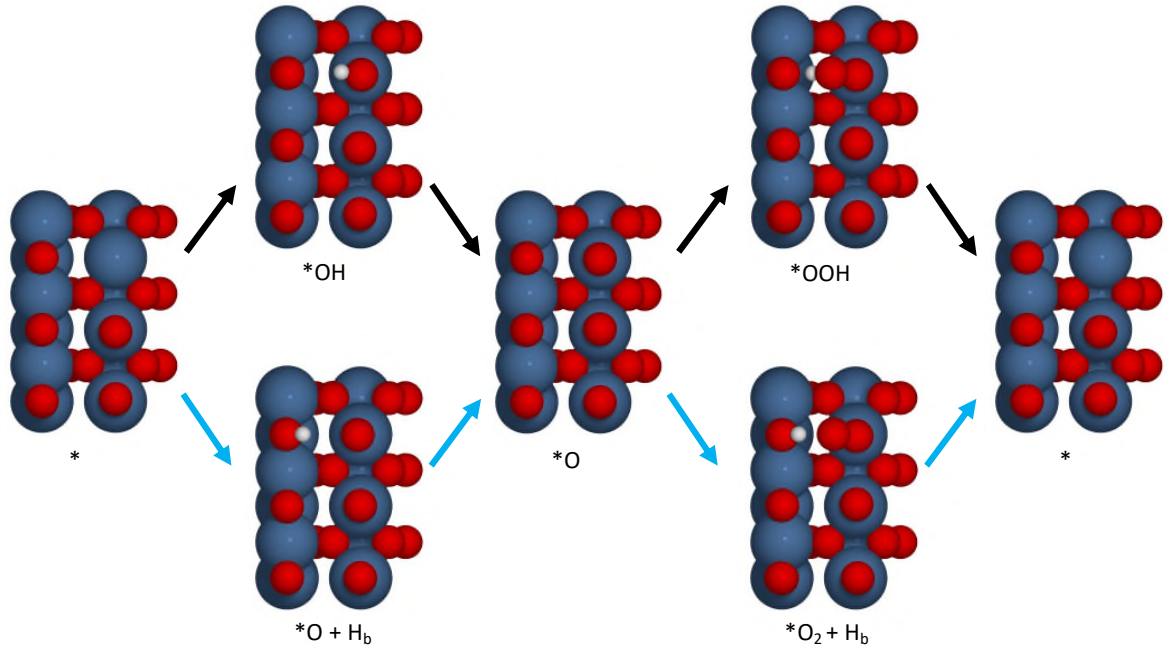

*Figure S18. OER reaction pathways considered in the DFT calculations, here shown on the rutile (110) surface of IrO_2. Black arrows indicate the conventional pathway while blue arrows indicate the alternative pathway where a hydrogen from *OH and *OOH is transferred to the neighboring bridging oxygen. Cus sites not acting as active site are covered by *O as expected to be the case close to the OER onset potential.*

References

(1) Baur, W. H.; Khan, A. A. Rutile-Type Compounds. IV. SiO2, GeO2 and a Comparison with Other Rutile-Type Structures. *Acta Crystallogr B* **1971**, *27* (11), 2133–2139. https://doi.org/10.1107/S0567740871005466.

(2) Owen, E. A.; Yates, E. L. XLI. Precision Measurements of Crystal Parameters. *The London, Edinburgh, and Dublin Philosophical Magazine and Journal of Science* **1933**, *15* (98), 472–488. https://doi.org/10.1080/14786443309462199.

(3) Wyckoff, R. W. G. *Crystal Structures - Volume 1*, 2nd ed.; Interscience Publishers: New York, 1963.

(4) Lejaeghere, K.; Van Speybroeck, V.; Van Oost, G.; Cottenier, S. Error Estimates for Solid-State Density-Functional Theory Predictions: An Overview by Means of the Ground-State Elemental Crystals. *Critical Reviews in Solid State and Materials Sciences* **2014**, *39* (1), 1–24. https://doi.org/10.1080/10408436.2013.772503.

(5) Bolzan, A. A.; Fong, C.; Kennedy, B. J.; Howard, C. J. Structural Studies of Rutile-Type Metal Dioxides. *Acta Crystallogr B* **1997**, *53* (3), 373–380. https://doi.org/10.1107/S0108768197001468.

(6) Talanov, A.; Phelan, W. A.; Kelly, Z. A.; Siegler, M. A.; McQueen, T. M. Control of the Iridium Oxidation State in the Hollandite Iridate Solid Solution K 1– x Ir 4 O 8. *Inorg Chem* **2014**, *53* (9), 4500–4507. https://doi.org/10.1021/ic5001667.

(7) Cairns, R. W.; Ott, E. X-Ray Studies of the System Nickel—Oxygen—Water. I. Nickelous Oxide and Hydroxide. *J Am Chem Soc* **1933**, *55* (2), 527–533. https://doi.org/10.1021/ja01329a013.

(8) Elliot, A. D. Structure of Pyrrhotite 5C (Fe9S1). *Acta Crystallogr B* **2010**, *66* (3), 271–279. https://doi.org/10.1107/S0108768110011845.

(9) Bestaoui, N.; Deniard, P.; Brec, R. Structural Study of a Hollandite-Type KxIrO2. *J Solid State Chem* **1995**, *118* (2), 372–377. https://doi.org/10.1006/jssc.1995.1356.

(10) Macrae, C. F.; Sovago, I.; Cottrell, S. J.; Galek, P. T. A.; McCabe, P.; Pidcock, E.; Platings, M.; Shields, G. P.; Stevens, J. S.; Towler, M.; Wood, P. A. Mercury 4.0: From Visualization to Analysis, Design and Prediction. *J Appl Crystallogr* **2020**, *53* (1), 226–235. https://doi.org/10.1107/S1600576719014092.

(11) El-Sayed, H. A.; Weiß, A.; Olbrich, L. F.; Putro, G. P.; Gasteiger, H. A. OER Catalyst Stability Investigation Using RDE Technique: A Stability Measure or an Artifact? *J Electrochem Soc* **2019**, *166* (8), F458–F464. https://doi.org/10.1149/2.0301908jes.